



# DNA-assisted synthesis of nanoceria, its size dependent structural and optical properties for optoelectronic applications

P S PRABHA JYOTHI<sup>1,2,\*</sup>, B ANITHA<sup>2</sup>, S SMITHA<sup>1,2</sup>, B V VIBITHA<sup>2</sup>, P G ANU KRISHNA<sup>2</sup>  
and NISHA J THARAYIL<sup>2</sup>

<sup>1</sup>Department of Physics, Sree Narayana College, Kollam 691001, India

<sup>2</sup>Department of Physics, Sree Narayana College for Women, Kollam 691001, India

\*Author for correspondence (prabhajyothi79@gmail.com)

MS received 14 January 2019; accepted 30 December 2019; published online 29 April 2020

**Abstract.** Cerium oxide ( $\text{CeO}_{2-x}$ ) nanoparticles or nanoceria were synthesized by the chemical co-precipitation method using cerium nitrate hexahydrate and ammonium carbonate as starting materials and deoxyribonucleic acid (DNA) as a capping agent. The structural and optical characterization of the prepared nanoparticles was studied in depth by X-ray diffraction (XRD), high resolution transmission electron microscopy (HRTEM), Fourier transform infrared spectroscopy, Raman spectroscopy, UV-visible absorption and diffuse reflectance spectroscopy. The average crystallite size and lattice parameters of the cerium oxide nanoparticles at different calcination temperatures were studied using XRD analysis. The average crystallite size was found to be 6 nm and the size increases with calcination temperature. The polycrystalline nature and the size of the particles obtained are in close agreement with HRTEM and Raman analysis. The optical band gaps of all samples were measured by Tauc plot which showed a blue shift with a decrease in size due to the quantum confinement effect. The optical absorption spectrum of the synthesized nanoparticles showed the absorption of UVA, UVB and UVC light, and the variation in structural and optical properties with size makes them suitable for the optoelectronic application. To the best of our knowledge, this is the first report on using DNA in the synthesis of nanostructured ceria.

**Keywords.** Nanostructured ceria; chemical co-precipitation; capping agent; DNA; optical studies.

## 1. Introduction

Cerium oxide, commonly known as ceria, is considered as a promising rare-earth oxide material due to its unique ability to toggle between  $\text{Ce}^{3+}$  and  $\text{Ce}^{4+}$  oxidation states depending on the oxygen partial pressure in the surrounding atmosphere. As a result, ceria can easily form nonstoichiometric compositions  $\text{CeO}_{2-x}$  with  $0 < x < 0.5$  without changing the crystal structure. Generally, cerium oxide has a cubic fluorite structure with space group  $Fm\bar{3}m$  [1]. It consists of a face-centred cubic unit cell of cerium cations with oxygen anions occupying the tetrahedral interstitial sites. The activity of cerium oxide particles increases when the size is shrunk down to nano-regime [2]. However, to enhance the properties of nanomaterials and thereby meet the need of different applications, it is very essential to decrease the size and thus to increase the active surface area of nanoparticles. In recent years, much effort has been focused on the development of new routes for the synthesis of nanoceria due to the range of applications in science and technology such as gas sensors, solar cells, high storage capacitor devices, fuel cells and UV filters [3–8]. Different synthetic methods are available for the fabrication of cerium oxide nanoparticles such as sol-gel, sonochemical, hydrothermal, chemical precipitation, combustion and pulsed laser deposition methods [9–13]. For various applications,

large-scale manufacturing of nano-powders needs to be cost effective, eco-friendlier and should not be too complex. Therefore, the chemical co-precipitation method is more attractive compared to others. As a better choice, the most fascinating biomaterial known to humans, deoxyribonucleic acid (DNA), has been used as a biological capping agent for the present study to obtain nanoparticles of very low dimensions with less aggregation. The use of capping agents prevents the growth of the particle by effectively shielding the surface of the nuclei as soon as they are formed. It prevents them from coming into direct contact with solution. Often, molecules with longer chains are used as capping agents. DNA is a polymer that carries genetic code of all living beings and it acts as a good capping agent as well as a template for nanomaterials using its double-helix nature [14]. So far, materials such as silver, gold, copper, palladium, platinum, carbon nanotubes and nickel oxide have been fabricated on the DNA template [14–17]. Moreover, there are no reports on the synthesis and characterization of nanoceria using DNA-assisted chemical co-precipitation. The structural features and optical properties of nanoceria have been studied in depth by using different characterization techniques such as X-ray diffraction (XRD), high-resolution transmission electron microscopy (HRTEM), Fourier transform infrared (FTIR), Raman and UV-visible spectroscopy.

## 2. Materials and method

### 2.1 Materials

Materials used: analytical grade cerium(III) nitrate hexahydrate ( $\text{Ce}(\text{NO}_3)_3 \cdot 6\text{H}_2\text{O}$ ) and ammonium carbonate ( $\text{NH}_4\text{HCO}_3 \cdot \text{NH}_2\text{COONH}_4$ ) were purchased from Merck; DNA powder was purchased from Sigma-Aldrich and the source of DNA powder was from calf thymus which has a B-DNA structure.

### 2.2 Experimental

Cerium oxide nanoparticles were synthesized by the chemical co-precipitation method by using 0.1 M aqueous solution of cerium nitrate hexahydrate and ammonium carbonate. They were added dropwise to the aqueous solution containing DNA powder as a capping agent under constant stirring. The mass of DNA was taken as equivalent to 0.01 M of ethylene diamine tetraacetic acid (EDTA) for comparison. Upon adding the solutions, cerium carbonate was precipitated. The major challenge often faced in the preparation of solution is the aggregation of nanostructures by Ostwald ripening and agglomeration [18]. This can be reduced by the use of capping agents. The steric hindrance of the double-helix DNA was considered as the preventing factor for the further growth of nanostructures. Due to the long polymeric chain of the DNA molecules there may be formation of a mesh-like network in the solution. The growth of the nanoparticles is blocked by the limited space in the network [17]. The whole mixture was then stirred for 5 h. After stirring, it was filtered and washed several times with deionized water. Then the dried carbonate precursor was calcined at 400, 500 and 600°C in a muffle furnace for 3 h. The synthesized cerium oxide nanoparticles were pale yellow in colour.

### 2.3 Characterization techniques

The crystalline phase of cerium oxide nanoparticles was determined by XRD of a Bruker AXS D8 Advance diffractometer using  $\text{CuK}\alpha$  radiation of wavelength 1.5406 Å in  $2\theta$  from 20° to 80° with a step size of 0.02°. The HRTEM analysis was performed using a Jeol/JEM 2100 instrument and the electron beam accelerating voltage was 200 kV. The optical absorbance of the cerium oxide nanoparticles was recorded using a Cary 5000 UV–Vis–NIR spectrophotometer in the wavelength range of 200–800 nm. The FTIR spectra of the specimen were recorded at room temperature on a Thermo-Fisher Scientific iS50 FTIR spectrophotometer in the transmittance mode. The micro-Raman spectra of the nano-material were recorded using a Labram-HR 800 spectrometer (Horiba Jobin Yvon) at an excitation wavelength of 633 nm.

## 3. Results and discussion

### 3.1 XRD analysis

Figure 1 shows the XRD pattern of the samples calcined at different temperatures. All the peaks are labelled and it is observed that they can be indexed with a pure cubic fluorite structure of  $\text{CeO}_{2-x}$  ( $0 < x < 0.5$ ) with lattice constant  $a = 5.420$  Å (JCPDS file no. 34-0394, space group  $Fm\bar{3}m$ ). The lattice constant of nanostructured ceria matches closely with that of silicon with a lattice constant of 5.431 Å. The sharp and strong diffraction pattern indicates the good crystallization of the prepared sample. No additional peak is observed, which reveals the high purity of the sample. The samples calcined at 400, 500 and 600°C are labelled CD1, CD2 and CD3.

The average crystallite size  $D$  can be estimated using the well-known Scherrer equation [19]:

$$D = 0.9\lambda / \beta \cos \theta \quad (1)$$

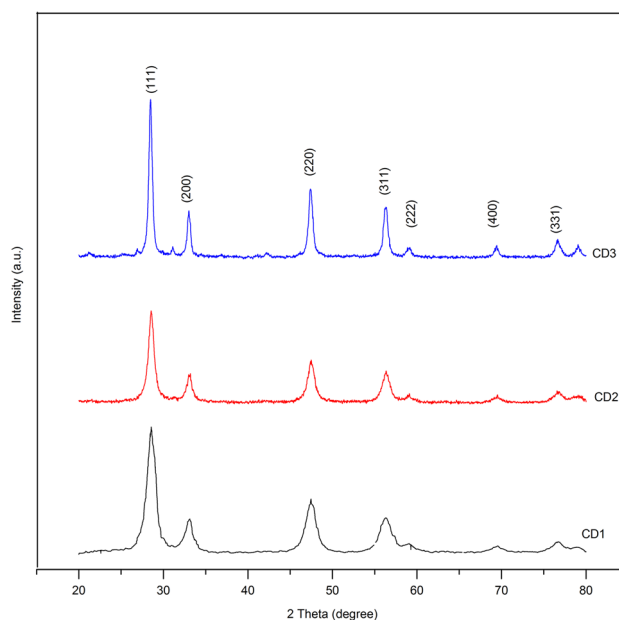


**Figure 1.** XRD pattern of  $\text{CeO}_{2-x}$  nanostructures synthesized at 400–600°C.

**Table 1.** Structural parameters obtained from analyses.

Sample code	Size from Scherrer equation (nm)	Lattice constant (Å)	Size from TEM analysis (nm)	Size from Raman analysis (nm)
CD1	$6 \pm 0.08$	5.4201	$6 \pm 2$	6.76
CD2	$9 \pm 0.27$	5.4108	$9 \pm 2$	10.06
CD3	$14 \pm 0.57$	5.4050	$16 \pm 2$	17.73

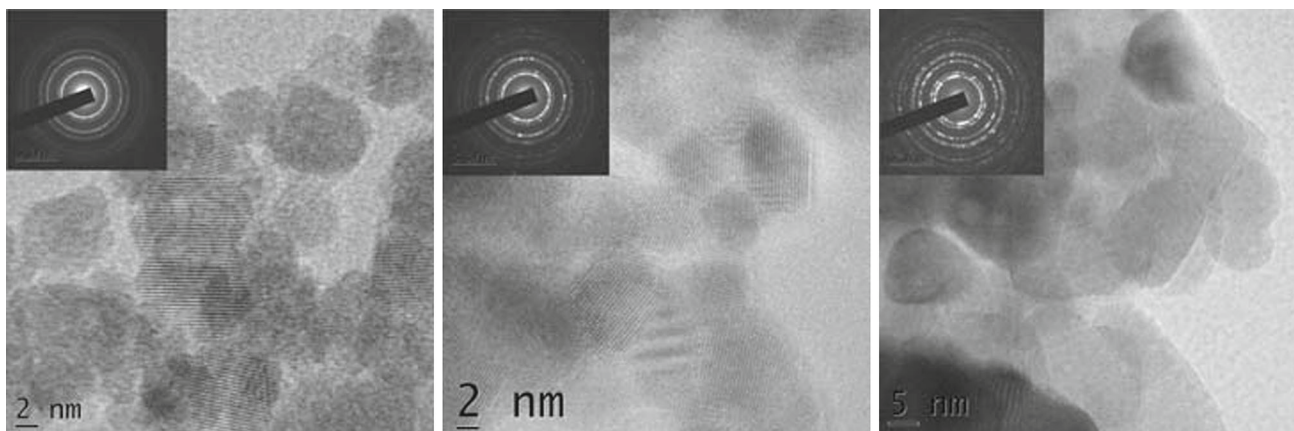


**Figure 2.** HRTEM images of the samples calcined at 400, 500 and 600°C.

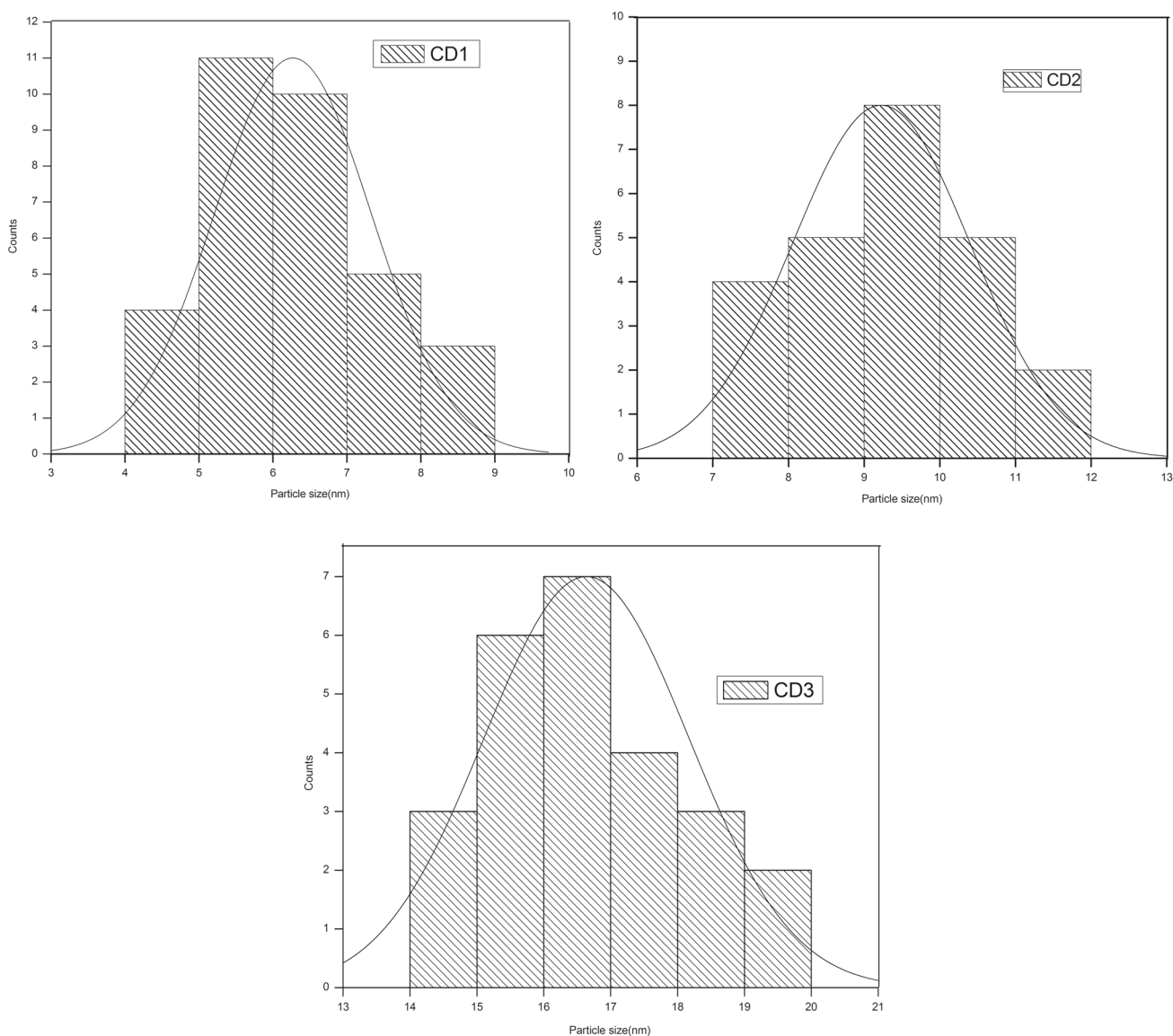


**Figure 3.** Size distribution of cerium oxide nanoparticles.

where  $\beta$  is the broadening of the  $(hkl)$  diffraction peak measured at half its maximum intensity,  $\lambda$  is the wavelength of the X-ray and  $\theta$  is the Bragg angle of the  $(hkl)$  peak.

Figure 1 shows that as calcination temperature increases, the diffraction peaks become intense and the full-width at half-maximum decreases. This indicates that crystallite size increases with temperature. The average crystallite size reported in this work is of significantly smaller than that reported in the earlier studies using the chemical capping agent, EDTA [20]. When the temperature increases, there is a decrease in defect concentration due to a decrease in the proportion of atoms. This improves the crystallinity of cerium oxide nanoparticles. Additionally, a decrease in the lattice constant was observed with an increase in crystallite size. Nanoparticles of oxide show a lattice expansion with a reduction in particle size. This can be attributed to an increase in vacancy or impurity concentrations [21]. When the cerium oxide is shrunk down to the nano-regime, structural defects get introduced due to oxygen vacancies in the lattice accompanied by the generation of  $Ce^{3+}$  species [2]. As the size reduces, the loss of even one oxygen anion creates a very high lattice strain. This strain in the lattice induces lattice expansion in order to relieve the strain [22]. When the  $Ce^{4+}$  ions reduce to  $Ce^{3+}$  ions, the number of  $O^{2-}$  anions decrease from eight to seven and thereby create disordered oxygen vacancies [23]. The ionic radius of  $Ce^{3+}$  (1.14 Å) is higher than that of  $Ce^{4+}$  (0.97 Å) [24]. Thus, the introduction of  $Ce^{3+}$  ions is also responsible for reduction in the lattice constant by introducing a change in inter-planar spacing [25]. Thus, the observations in the present study are in good agreement with earlier reports. Moreover, it is also observed that nanostructured ceria has a strong tendency to remain in the cubic fluorite structure even after losing  $O^{2-}$  anions. Table 1 shows the average size and lattice constant of the prepared samples using XRD, TEM and Raman analysis.

### 3.2 TEM analysis

The morphology, particle size and crystallinity of the samples were characterized by HRTEM. Figure 2 shows the HRTEM images of nanoceria calcined at 400, 500 and 600°C with selected area electron diffraction (SAED) pattern in the inset. The size distribution is plotted in the histograms as shown in figure 3. The average particle size obtained from the images are about  $6 \pm 2$ ,  $9 \pm 2$  and  $16 \pm 2$  nm, respectively, which are in good agreement with the results deduced from the XRD analysis. The image reveals that the particles are not exactly spherical in shape. Debye ring obtained in the SAED patterns confirms the polycrystalline nature of cerium oxide nanoparticles. With a polycrystalline specimen of random orientation, a Debye ring is formed, because the normal to any set of  $(hkl)$  planes have all possible orientations in space [19,21]. Agglomeration of nanoparticles is very common because they try to decrease the exposed surface area for lowering the surface energy. Thus, among the nanoparticles,

the smaller particles have strong agglomeration. In the present study, we are able to reduce the aggregation to a great extent by the use of DNA. In the double-stranded structure, the sugar phosphate backbones follow a helical path and the bases are in the helical array in the central core. The four bases in the DNA include adenine, thymine, guanine and cytosine. Each turn of the helical structure produces one major and minor groove [17]. Based on this structural mode, major groove of the DNA is the suitable place for the nanoparticles growth where the space is large enough to accommodate nanoparticles. The nucleation may occur, first starting from the cerium ions bound on the DNA base or the phosphate groups, and then the cerium ions are slowly reduced on the nucleation site. The growth of the nanoparticles is finally blocked by the major groove of DNA. The oxidation process can

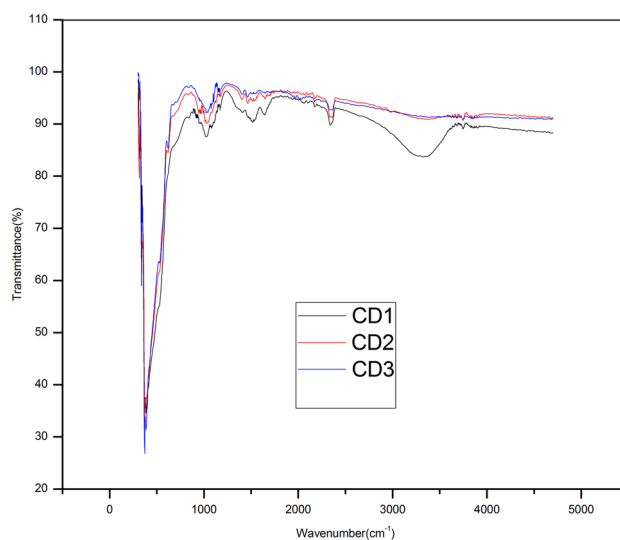


Figure 4. FTIR spectrum of cerium oxide nanoparticles.

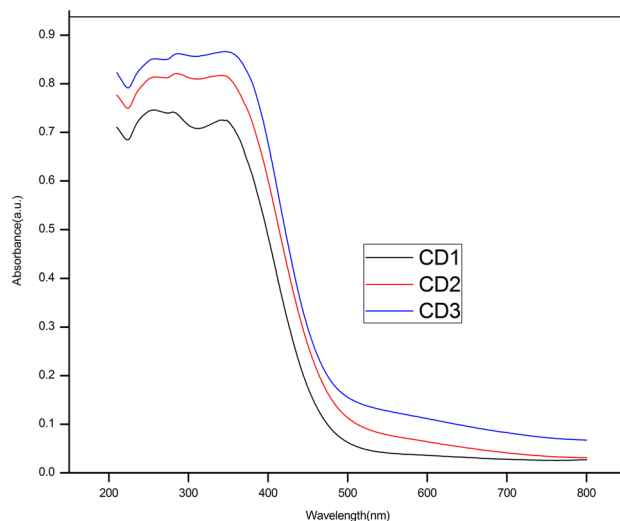


Figure 5. UV-visible absorbance spectra of ceria nanoparticles.

occur there and finally produce cerium oxide nanoparticles [16,26]. The groove binding and electrostatic interaction of a molecule with DNA show less or no perturbations on the base stacking and helicity bands because these two binding modes do not influence the secondary structure of the DNA [27,28].

### 3.3 FTIR spectra

FTIR spectra of the samples in the transmission mode are presented in figure 4. The spectra have several absorption peaks recorded from 4000 to 400  $\text{cm}^{-1}$  and the broad peak at 3300  $\text{cm}^{-1}$  corresponds to the O–H stretching vibrations present in the water molecules [29] and are clearly attenuated as the calcination temperature increases. Under an ambient atmosphere, carbonation of nanoceria is unavoidable and the weak absorption band at around 1510  $\text{cm}^{-1}$  corresponds

to the O–C–O stretching band [8]. Furthermore, the weak absorption region from 950 to 1150  $\text{cm}^{-1}$  is associated with symmetric and asymmetric stretching of the phosphate group in the nucleic acid residuals [30]. The Ce–O stretching vibrations can be identified around 450  $\text{cm}^{-1}$ , which confirms the formation of cerium oxide molecule [31].

### 3.4 UV–visible spectra

Absorption spectra of particles were recorded using a UV–visible spectrophotometer. The absorption of UV–visible light may result in the excitation of electrons to higher energy states. The spectrum of nanoceria (figure 5) shows a broad absorption band. It exhibits a strong absorption band below 400 nm in the UV region due to a charge transfer transition from oxygen 2p to cerium 4f which is a direct recombination of the electrons in the  $\text{Ce}^{4+}$  (4f) conduction band with the

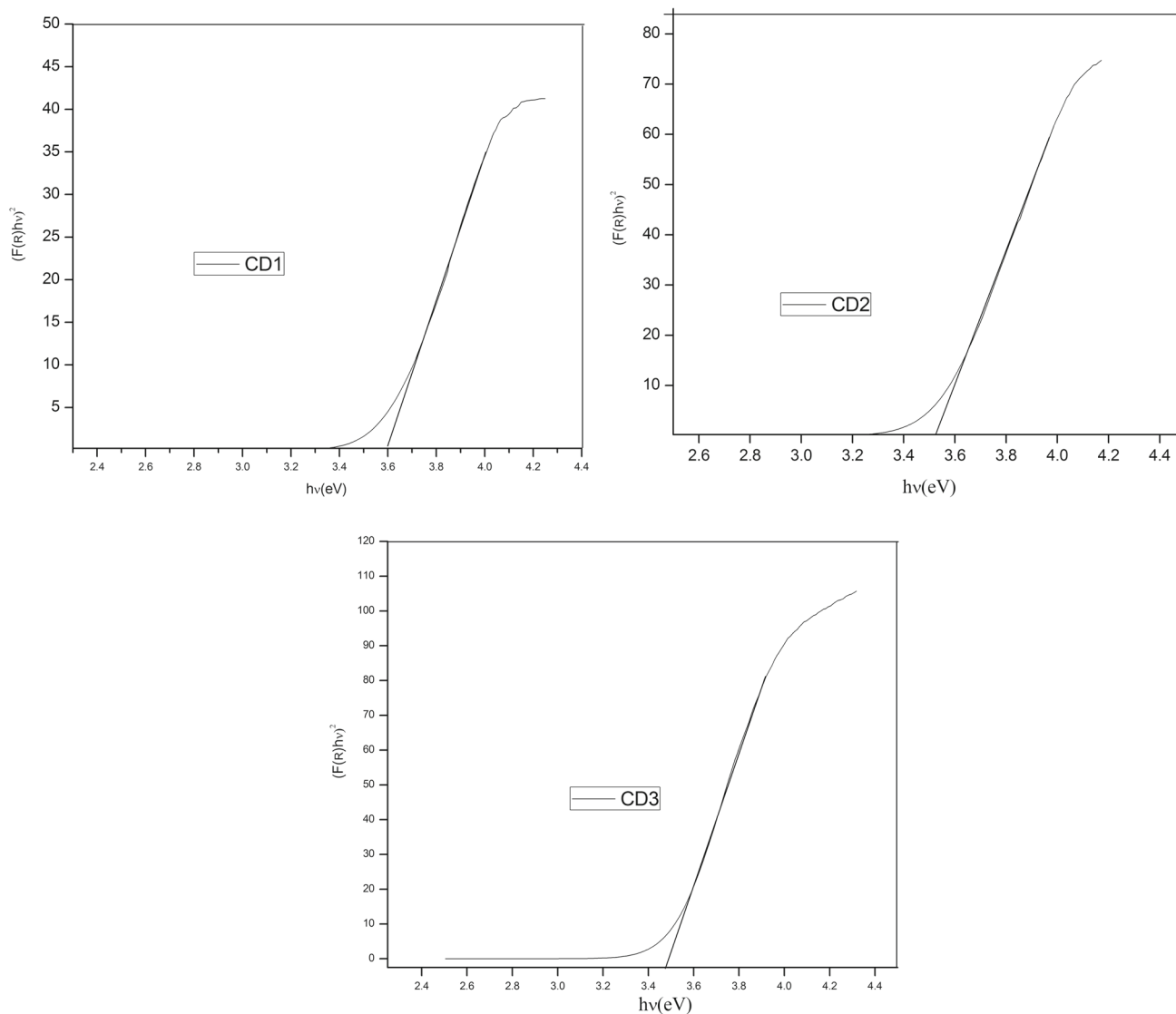


**Figure 6.** Tauc plot of cerium oxide nanoparticles calcined at 400, 500 and 600°C.

holes in the  $O^{2-}$  (2p) valence band [32]. From the spectrum, it is clear that DNA-assisted synthesized nanocerium can filter UVA (320–400 nm), UVB (290–320 nm) and UVC (200–290 nm) light. For the filtration of UVA, the availability of a suitable inorganic material is limited. The present investigation reveals that DNA-assisted synthesized nanocerium, with no known toxicity, is a promising candidate as an inorganic UV filter. Furthermore, it has very good transparency over visible light.

The optical band gap,  $E_g$ , of the sample can be determined using the following equation:

$$F(R)h\nu = A(h\nu - E_g)^n \quad (2)$$

where  $F(R)$  is calculated from the Kubelka–Munk relation [32–34],  $h\nu$  is the photon energy,  $A$  is a constant and  $n$  can have values 1/2, 3/2, 2 and 3 depending on the mode of inter-band transition. The direct optical band gap is determined by extrapolating the linear portion of the curve  $(F(R)h\nu)^2$  vs.  $(h\nu)$  to zero absorption (Tauc plot) as shown in figure 6.

The energy band gap values obtained for CD1, CD2 and CD3 are 3.59, 3.52 and 3.47 eV which are higher than those of bulk cerium oxide particles (3.15 eV) [35–37]. The energy band gap increases as the size of the nanoparticle decreases. It confirms a blue shift for the nanoparticles due to the quantum confinement effect. The quantum size confinement effect becomes significant particularly when the particle size becomes comparable to or smaller than the Bohr exciton radius [38]. It implies that we can tune the optical properties of these nanoparticles as per our wish to utilize them for the next-generation optoelectronic devices since they have high thermal stability, and their lattice constant as well as band gap match well with those of silicon. These are the essential characteristics for the application of silicon-like structures.

### 3.5 Raman spectra

Raman spectra of cerium oxide nanoparticle samples are shown in figure 7. The spectra were recorded using an excitation wavelength of 633 nm and active modes obtained were 461.35, 462.23 and 463.99  $cm^{-1}$  for samples calcined at 400, 500 and 600°C, respectively. The single Raman band observed in the spectra confirms the fluorite-type cubic crystal structure of cerium oxide nanoparticles that exhibits only one allowed Raman mode. The band emanates from the symmetric breathing vibrational mode of the oxygen ions around each cation [39]. Thus, this mode should be very sensitive to any disorder in the oxygen sub-lattice [40]. As the calcination temperature increases there is a shift in the Raman band to higher wavenumber side. This may be due to the change of bond length due to lattice distortion or any disorder in the oxygen sub-lattice [41]. The shift in the Raman

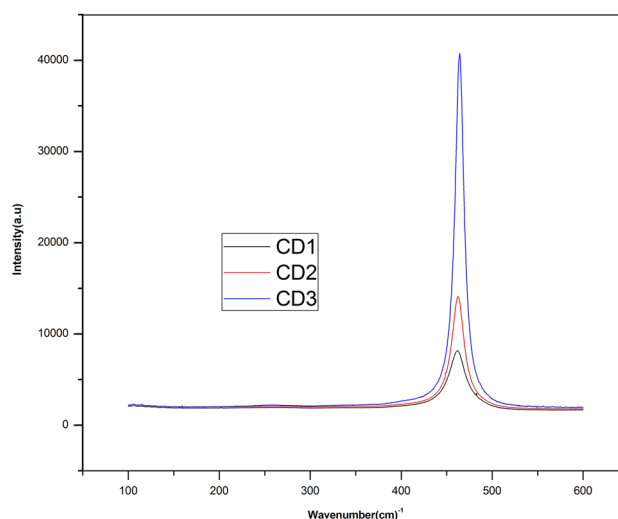


**Figure 7.** Raman spectra of  $CeO_{2-x}$  nanoparticles.

peak towards the lower wavenumber side compared to its bulk form indicates that the synthesized samples are in the nano-regime. The shifting of the peak due to the particle size effect is a noteworthy character in determining the different properties of nanomaterials [42]. It is also observed that the intensity of the peak increases as the calcination temperature increases. The particle size of the sample can be calculated from Raman line broadening using equation (3):

$$\Gamma \text{ (cm}^{-1}\text{)} = 10 + 124.7/D \quad (3)$$

where  $\Gamma \text{ (cm}^{-1}\text{)}$  is the full-width at half-maximum of the Raman active mode and  $D$  is the particle size of the nano-structure [43].

The particle sizes calculated from equation (3) are 6.76, 10.07 and 17.76 nm for CD1, CD2 and CD3, respectively. This calculated particle size is almost closer to the values determined from XRD analysis and consistent with the TEM results.

## 4. Conclusions

The DNA-assisted chemical co-precipitation method has been successfully used for the preparation of nanostructured cerium oxide particles. The average crystallite size of the particle is found to be 6 nm and it increases with an increase in the calcination temperature. The results obtained from XRD, HRTEM and Raman analyses are in close agreement with each other and confirm the polycrystalline nature of cerium oxide nanoparticles. Lattice expansion is observed with a decrease in the calcination temperature without changing the cubic fluorite structure. It is due to the oxygen vacancies and introduction of  $Ce^{3+}$  ions into the lattice. The FTIR spectra

reveal the purity of the nanoparticles. The optical band gaps increase with a decrease in size which indicates that there is blue shift for the nanoparticles. The blue shift reported in optical studies concludes a strong quantum confinement effect. The present investigation reveals that DNA-assisted synthesized ceria nanoparticles are promising materials as an inorganic filter for UVA, UVB and UVC light. We can tune the optical properties of these nanoparticles, and also their lattice constant as well as band gap match well with those of silicon. Moreover, the observed structural and optical properties of nanoceria make it a suitable candidate for next-generation optoelectronic devices.

### Acknowledgements

The authors acknowledge SAIF, Cochin and CLIF University of Kerala for providing facilities for characterization.

### References

- [1] Mogensen M, Sammes N M and Tompsett G A 2000 *Solid State Ion.* **129** 63
- [2] Ma Y, Gao W, Zhang Z, Zhang S, Tia Z, Liu Y *et al* 2018 *Surface Sci. Rep.* **73** 1
- [3] Garzon F H, Mukundan R and Brosha E L 2000 *Solid State Ion.* **633** 136
- [4] Dimonte R, Fornasiero P, Graziani M and Kašpar J 1998 *J. Alloys Compd.* **877** 275
- [5] Elidrissi B, Addou M, Regragui M, Monty C, Bougrine A and Kachouane A 2000 *Thin Solid Films* **379** 23
- [6] Zivkovi L S, Lair V, Lupan O and Ringued A 2011 *Russ. J. Phys. Chem.* **85** 2358
- [7] Lin H C 2005 *Hydrometall. China* **24** 9
- [8] Devadoss M D, Prabaharan M, Sadaiyandi K, Mahendran M and Sagadevan S 2016 *Mater. Res.* **19** 478
- [9] Xiao H, Ai Z and Zhang L 2009 *J. Phys. Chem.* **113** 16625
- [10] Yin L, Wang Y, Pang G, Kolytyn Y and Gedanken A 2002 *J. Colloid Interface Sci.* **246** 78
- [11] Anushree S and Kumar C 2015 *Mater. Chem. Phys.* **155** 223
- [12] Purohit R D, Sharma B P, Pillai K T and Tyagi A K 2001 *Mater. Res. Bull.* **36** 2711
- [13] Alla S K, Mandal R K and Prasad N K 2016 *RSC Adv.* **105** 102821
- [14] Liu Z, Zu Y, Fu Y, Zhang Y and Liang H 2008 *Mater. Lett.* **62** 2315
- [15] Braun E, Eichen Y, Sivan U and Ben Yoseph G 1998 *Nature* **391** 775
- [16] Yao Y, Song Y and Wang L 2008 *Nanotechnology* **19** 405601
- [17] Nithyaja B, Misha H and Nampoori V P N 2012 *Nano Sci. Nanotechol.* **2** 99
- [18] Cao G 2004 *Nano structures and nano materials* (London: Imperial College Press)
- [19] Cullity B D 2001 *Elements of X-ray diffraction* 3rd edn (New Jersey: Prentice Hall)
- [20] Priyanka K P, Babitha K, Sreedevi A, Sheena X, Mohammed E M and Varghese T 2014 *J. Electroceram.* **32** 361
- [21] Suryanarayana C and Grant Norton M 1998 *X-ray diffraction – a practical approach* (New York: Plenum Press)
- [22] Deshpande S, Patil S, Kuchibhatla S V N T and Seal S 2005 *Appl. Phys. Lett.* **87** 133113
- [23] Maksimchuk O, Masalov A A and Malyukin Yu V 2013 *J. Nano-Electron. Phys.* **5** 01004-1
- [24] Goharshadi E K and Paul S S 2011 *J. Colloid Interface Sci.* **356** 473
- [25] Phokha S, Pinitsoontorn S, Chirawatkul P, Pooarporn Y and Maensiri S 2012 *Nanoscale Res. Lett.* **7** 425
- [26] Li Q, Wang L, Hu B, Yang C, Zhou L and Zhang L 2007 *Mater. Lett.* **61** 1615
- [27] Jackson B A, Alekseyev V Y and Barton J K 1999 *Biochemistry* **38** 4655
- [28] Nina K, Mikhail V, Eugenii I, Evgenii T, Roman B, Petr S *et al* 2016 *J. Nanomat.* **2016** 12
- [29] Tan H R, Tan J P Y, Boothroyd C, Hansen T W, Foo Y L and Lin M J 2012 *J. Phys. Chem.* **116** 242
- [30] Han Y, Han L, Yao Y, Li Y and Liu X 2018 *Anal. Methods* **10** 2436
- [31] Deus R C, Foschini C R, Spitova B, Moura F, Longo E and Simoes A Z 2014 *Ceram. Int.* **40** 1
- [32] Soni S, Kumar S, Dalela B, Kumar S, Alvi P A and Dalela S 2018 *J. Alloys Compd.* **752** 520
- [33] Kubelka P and Munk F 1931 *Tech. Phys.* **12** 593
- [34] Abdullahi S S, Guner S, Koseoglu Y, Musa I M, Adamu B I and Abdulhamid M I 2016 *J. NAMP* **35** 241
- [35] Blitz J P 1998 *Modern techniques in applied molecular spectroscopy* (John Wiley & Sons, Inc.)
- [36] Phoka S, Laokul P, Swatsitang E, Promarak V, Seraphin S and Maensiri S 2009 *Mater. Sci. Eng.* **115** 423
- [37] Arul N S, Mangalaraj D, Chen P C, Ponpandian N and Viswanathan C 2011 *Mater. Lett.* **65** 2635
- [38] Zhang J Z 2009 *Optical properties and spectroscopy of nano-materials* (World Scientific Publishing Co. Pvt. Ltd.)
- [39] Mazali I O, Viana B C, Alves O L, Filho J M and Souza Filho A G 2007 *J. Phys. Chem. Solids* **68** 622
- [40] Radovic M, Dohcevic-Mitrovic Z, Scepanovic M, Grujic-Brojcin M, Matovic B, Boskovic S *et al* 2007 *Sci. Sin.* **39** 281
- [41] Hattori T, Kobayashi K and Ozawa M 2017 *Jpn. J. Appl. Phys.* **56** 06
- [42] Jiang Q, Shi H X and Zhao M 1999 *J. Chem. Phys.* **111** 2176
- [43] Kumar S, Srivastava M, Singh J, Layek S, Yashpal M, Materny A *et al* 2015 *AIP Adv.* **5** 027109